GeoStruct Innovations
https://www.acadlore.com/journals/GSI

Natural Frequency Analysis of Functionally Graded Porous Beams Using Hyperbolic Shear Deformation Theory

Burak İkinci[1*], Lazreg Hadji[2], Mehmet Avcar[1]

[1] Department of Civil Engineering, Faculty of Engineering and Natural Sciences, Suleyman Demirel University, 32260 Cunur, Turkey
[2] Department of Civil Engineering, University of Tiaret, BP 78 Zaaroura, 14000 Tiaret, Algeria

* Correspondence: Burak İkinci (burakikinci@sdu.edu.tr)

Received: 07-12-2024 **Revised:** 09-04-2024 **Accepted:** 09-20-2024

Citation: B. İkinci, L. Hadji, and M. Avcar, "Natural frequency analysis of functionally graded porous beams using hyperbolic shear deformation theory," *GeoStruct. Innov.*, vol. 2, no. 3, pp. 125–134, 2024. https://doi.org/10.56578/gsi020302.

Abstract: The free vibration characteristics of functionally graded porous (FGP) beams were investigated through the application of hyperbolic shear deformation theory (HSDT). The material properties were described using a modified rule of mixtures, incorporating the porosity volume fraction to account for various porosity distribution types, enabling the continuous variation of properties across the beam thickness. The kinematic relations for FGP beams were formulated within the framework of HSDT, and the governing equations of motion were derived using Hamilton's principle. Analytical solutions for free vibration under simply supported boundary conditions were obtained using Navier's method. Validation was conducted through comparisons with existing data, demonstrating the accuracy and reliability of the proposed approach. The effects of porosity distribution patterns, power-law indices, span-to-depth ratios, and vibrational mode numbers on the natural frequency values of FGP beams were comprehensively examined. The findings provide critical insights into the influence of porosity and geometric parameters on the dynamic behavior of functionally graded (FG) beams, offering a robust theoretical foundation for their design and optimization in advanced engineering applications.

Keywords: Free vibration; Hyperbolic shear deformation; Functionally graded materials; Porosity

1 Introduction

FG materials (FGMs) have drawn a lot of attention lately because of their special qualities and possible uses in a variety of engineering fields, such as mechanical, civil, and aerospace engineering. FG beams combine the advantageous qualities of several materials to provide better performance, which makes them particularly suitable for use in load-bearing structures exposed to dynamic loading conditions [1–3].

Porosity may occur due to defects or thermal differences. In other situations, the porosity of FGM is the desired result of its unique abilities [4, 5]. Imitating nature to possess abilities, FGP materials possess distinct advantages, enabling their usage in various engineering applications. The unique mechanical properties of porous FGMs, which are derived from gradation in material composition and porosity, allow them to exhibit superior strength-to-weight ratios and enhanced energy absorption capabilities. These characteristics are precious in fields such as aerospace engineering, where reducing weight while maintaining structural integrity is crucial for performance and fuel efficiency. The ability to tailor material properties, including stiffness and damping characteristics, through the design of the porosity distribution provides engineers with innovative solutions to address specific operational demands [6–16].

Additionally, in civil engineering, FGP beams can be employed in lightweight structural components, such as bridges and high-rise buildings, where controlling vibrations is vital for the safety and comfort of occupants [17–19]. The vibration behavior of beams is an essential part of structural analysis because it provides insights into the stability and safety of engineering structures. Traditional beam theories often assume idealized conditions that do not account for shear deformations or variations in material properties. However, as the dimensions of structural elements decrease—particularly in modern engineering applications—shear deformations become increasingly significant.

Therefore, it is essential to explore the dynamic behavior of FGP beams with HSDT to design safer and more effective structural elements [20, 21].

This study presents an analysis of the free vibration characteristics of FGP beams via HSDT. A refined beam theory that accounts for both shear deformations and the effects of porosity was employed, aiming to provide more accurate predictions of natural frequencies and mode shapes. This study seeks to enhance the understanding of the vibrational behavior of these advanced materials and evaluate the influence of various parameters, including material grading and porosity distribution, on their dynamic performance.

The results of this study can have practical consequences for the design and usage of FGP beams in engineering practice, in addition to advancing the theoretical understanding of their free vibration.

2 Methodology

2.1 Model of the FGP Beam

A straight functionally graded porous (FGP) beam with a rectangular cross-section, characterized by its length L, width b, and thickness h, was considered in the present study. The beam is assumed to be simply supported at both ends. The Cartesian coordinate system O(x, y, z) is located on the left edge of the central axis of the beam, where x-, y-, and z-axes are taken along the length, width and depth of the beam, as given in Figure 1.

An FG beam is composed of ceramic and metal constituents, where material composition at the upper surface is assumed to be ceramic-rich and varies continuously to the metal-rich one located in the lower surface. Besides, an FGP beam is supposed to include porosities spreading across thickness because of the fault during manufacture and this situation is described with even (IP-I) and uneven (IP-II) porosity models in the study by Wattanasakulpong and Chaikittiratana [22], as shown in Figure 1.

The modified rule of mixture for an FGP beam with a porosity volume fraction, $\alpha(\alpha \ll 1)$, can be expressed [22]:

$$P = P_m \left(V_m - \frac{\alpha}{2}\right) + P_c \left(V_c - \frac{\alpha}{2}\right) \tag{1}$$

where, P_m and P_c are the material properties of metal and the ceramic; and V_m and V_c are their volume fractions, respectively.

The relation for the total volume fraction of the metal and ceramic constituents is:

$$V_m + V_c = 1 \tag{2}$$

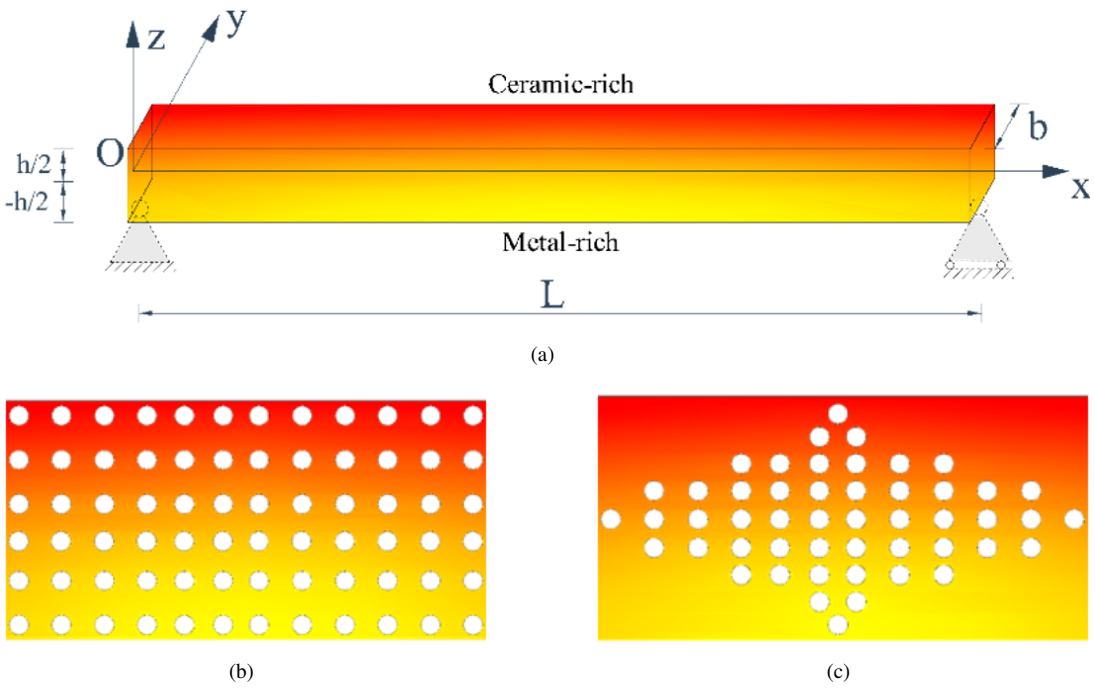

Figure 1. (a) The geometry; (b) even (IP-I) porosity distribution; (c) uneven (IP-II) porosity distribution of the FG beam

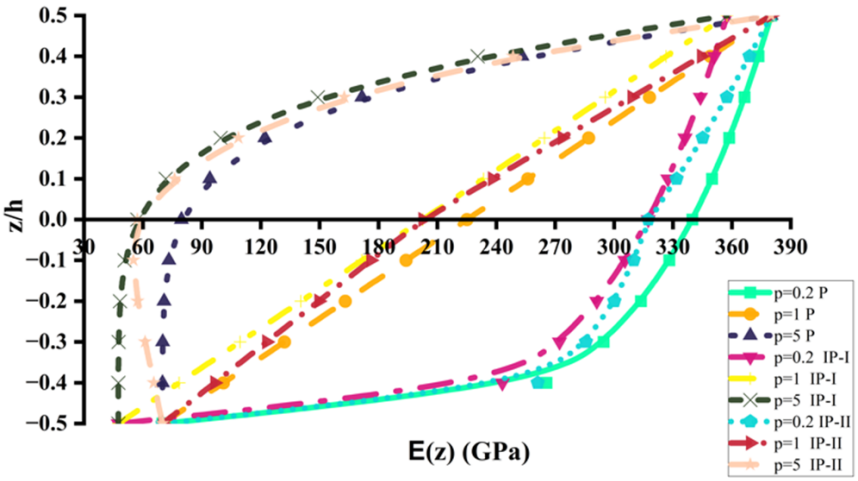

Figure 2. Variation of Young's modulus of the FG beams with IP-I vs IP-II porosity distributions across the thickness direction

The volume fraction of the ceramic constituents obeys the following power-law function for FGP beams:

$$V_c = \left(\frac{z}{h} + \frac{1}{2}\right)^p \tag{3}$$

where, p denotes the power-law index $(0 \leq p \leq \infty)$, and z is the distance from the mid-plane of the FG beam.

The effective material properties of FGP beams with even (IP-I) and uneven (IP-II) porosity models can be expressed as follows, respectively [22]:

$$P = (P_c - P_m)\left(\frac{z}{h} + \frac{1}{2}\right)^p + P_m - \frac{\alpha}{2}(P_c + P_m) \tag{4}$$

$$P = (P_c - P_m)\left(\frac{z}{h} + \frac{1}{2}\right)^p + P_m - \frac{\alpha}{2}(P_c + P_m)\left(1 - \frac{2|z|}{h}\right) \tag{5}$$

It can be noted that, as $\alpha = 0$, the FG beam becomes the perfect one. In this case, as p=0, the FG beam becomes a fully ceramic one, while it turns into a fully metal one for p=∞.

In this study, unless otherwise indicated, FG beams are composed of aluminum (Al) as the metal phase and alumina (Al_2O_3) as the ceramic phase. The material properties are as follows: E_m=70 GPa; ρ_m=2702 kg/m^3; E_c=380 GPa; and ρ_c=3960 kg/m^3. Figure 2 illustrates the variations of Young's modulus of FG beams with P, IP-I, and IP-II models across the thickness direction.

2.2 Governing Equations

2.2.1 Basic assumptions

Bending (w_b) and shear (w_s) are two of the components that make up the transverse displacements. Only x and t have any effect on these components.

$$w(x, z, t) = w_b(x, t) + w_s(x, t) \tag{6}$$

The axial displacement is made up of extension, bending, and shear components as follows:

$$u = u_0 + u_b + u_s \tag{7}$$

The displacements of the bending component, w_b, are considered the same as the displacements given by the classical beam theory. Hence, u_b can be described as:

$$u_b = -z\frac{\partial w_b}{\partial x} \tag{8}$$

In combination with w_s, the shear component (u_s) produces a variation in shear strain (γ_{xz}) and hence in shear stress (τ_{xz}) over the thickness of the beam. Therefore, shear stress (τ_{xz}) is zero at the top and bottom faces of the FG beam. As a result, the expression for u_s may be written as:

$$u_s = -f(z)\frac{\partial w_s}{\partial x} \tag{9}$$

where, $f(z)$ is defined as a hyperbolic function [23]:

$$f(z) = z\left[1 + \frac{3\pi}{2}\operatorname{sech}^2\left(\frac{1}{2}\right)\right] - \frac{3\pi}{2}h\tanh\left(\frac{z}{h}\right) \tag{10}$$

2.2.2 Kinematics and constitutive equations

The field of displacement of the HSDT can be constructed based on the assumptions established in the earlier section as follows:

$$u(x,z,t) = u_0(x,t) - z\frac{\partial w_b}{\partial x} - f(z)\frac{\partial w_s}{\partial x} \tag{11}$$

$$w(x,z,t) = w_h(x,t) + w_s(x,t) \tag{12}$$

The displacements are related to the following strains:

$$\varepsilon_x = \varepsilon_x^0 + zk_x^b + f(z)k_x^s \tag{13}$$

and

$$\gamma_{xz} = g(z)\gamma_{xz}^s \tag{14}$$

where,

$$\varepsilon_x^0 = \frac{\partial u_0}{\partial x}, k_x^b = -\frac{\partial^2 w_b}{\partial x^2}, k_x^s = -\frac{\partial^2 w_s}{\partial x^2} \tag{15}$$

$$g(z) = 1 - \frac{df(z)}{dz} \tag{16}$$

According to Hooke's law,

$$\sigma_x = Q_{11}(z)\varepsilon_x \text{ and } \tau_{xz} = Q_{55}(z)\gamma_{xz} \tag{17}$$

where,

$$Q_{11}(z) = E(z) \text{ and } Q_{55}(z) = \frac{E(z)}{2(1+v)} \tag{18}$$

2.2.3 Equations of motion

Hamilton's principle was used to develop the equations of motion [24]:

$$0 = \int_0^t (\delta U - \delta K)dt \tag{19}$$

where, $t, \delta U$ and δK are the time and the virtual variations of the strain kinetic energy.

The variation in the strain energy of the beam may be represented as:

$$\begin{aligned}\delta U &= \int_0^L \int_{-\frac{h}{2}}^{\frac{h}{2}} \left(\sigma_x \delta\varepsilon_x + \tau_{xz}\delta\gamma_{xz}\right) dzdx \\ &= \int_0^L \left(N\frac{d\delta u_0}{dx} - M_b\frac{d^2\delta w_b}{dx^2} - M_s\frac{d^2\delta w_s}{dx^2} + Q_{xz}\frac{d\delta w_s}{dx}\right) dx\end{aligned} \tag{20}$$

where, the stress resultants N, M_b, M_s and Q_{xz} are specified as:

$$(N, M_b, M_s) = \int_{-\frac{h}{2}}^{\frac{h}{2}} (1, z, f)\sigma_x dz \tag{21}$$

The variation in kinetic energy may be represented as:

$$\begin{aligned}
\delta K &= \int_0^L \int_{-\frac{h}{2}}^{\frac{h}{2}} \rho(z)[\dot{u}\delta\dot{u} + \dot{w}\delta\dot{w}]dzdx \\
&= \int_0^L \left\{ I_0 \left[\dot{u}_0\delta\dot{u}_0 + (\dot{w}_b + \dot{w}_s)\left(\delta\dot{w}_b + \delta\dot{w}_s\right)\right] - I_1\left(\dot{u}_0\frac{d\delta\dot{w}_b}{dx} + \frac{d\dot{w}_b}{dx}\delta\dot{u}_0\right)\right. \\
&\quad + I_2\left(\frac{d\dot{w}_b}{dx}\frac{d\delta\dot{w}_b}{dx}\right) - J_1\left(\dot{u}_0\frac{d\delta\dot{w}_s}{dx} + \frac{d\dot{w}_s}{dx}\delta\dot{u}_0\right) + K_2\left(\frac{d\dot{w}_s}{dx}\frac{d\delta\dot{w}_s}{dx}\right) \\
&\quad \left. + J_2\left(\frac{d\dot{w}_b}{dx}\frac{d\delta\dot{w}_s}{dx} + \frac{d\dot{w}_s}{dx}\frac{d\delta\dot{w}_b}{dx}\right)\right\} dx
\end{aligned} \tag{22}$$

where, the differentiation with respect to the time variable t is indicated by the dot-superscript convention; $\rho(z)$ is the mass density; and $(I_0, I_1, J_1, I_2, J_2, K_2)$ are the mass inertia and specified as:

$$(I_0, I_1, J_1, I_2, J_2, K_2) = \int_{-\frac{h}{2}}^{\frac{h}{2}} \left(1, z, f, z^2, zf, f^2\right)\rho(z)dz \tag{23}$$

The following equations of motion of the FG beam were found by substituting Eqs. (21) and (23) into Eq. (20), gathering the coefficients of $\delta u_0, \delta w_b$, and δw_s, and integrating by parts vs. both spatial and time variables:

$$\delta u_0 : \frac{dN}{dx} = I_0\ddot{u}_0 - I_1\frac{d\ddot{w}_b}{dx} - J_1\frac{d\ddot{w}_s}{dx} \tag{24}$$

$$\delta w_b : \frac{d^2M_b}{dx^2} = I_0\left(\ddot{w}_b + \ddot{w}_s\right) + I_1\frac{d\ddot{u}_0}{dx} - I_2\frac{d^2\ddot{w}_b}{dx^2} - J_2\frac{d^2\ddot{w}_s}{dx^2} \tag{25}$$

$$\delta w_s : \frac{d^2M_s}{dx^2} + \frac{dQ}{dx} = I_0\left(\ddot{w}_b + \ddot{w}_s\right) + J_1\frac{d\ddot{u}_0}{dx} - J_2\frac{d^2\ddot{w}_b}{dx^2} - K_2\frac{d^2\ddot{w}_s}{dx^2} \tag{26}$$

Eqs. (13)-(16), (17)-(18), and (21) may be used to formulate Eqs. (24)-(26) in terms of displacements (u_0, w_b, w_s) as follows:

$$A_{11}\frac{\partial^2 u_0}{\partial x^2} - B_{11}\frac{\partial^3 w_b}{\partial x^3} - B_{11}^s\frac{\partial^3 w_s}{\partial x^3} = I_0\ddot{u}_0 - I_1\frac{d\ddot{w}_b}{dx} - J_1\frac{d\ddot{w}_s}{dx} \tag{27}$$

$$B_{11}\frac{\partial^3 u_0}{\partial x^3} - D_{11}\frac{\partial^4 w_b}{\partial x^4} - D_{11}^s\frac{\partial^4 w_s}{\partial x^4} = I_0\left(\ddot{w}_b + \ddot{w}_s\right) + I_1\frac{d\ddot{u}_0}{dx} - I_2\frac{d^2\ddot{w}_b}{dx^2} - J_2\frac{d^2\ddot{w}_s}{dx^2} \tag{28}$$

$$\delta B_{11}^s\frac{\partial^3 u_0}{\partial x^3} - D_{11}^s\frac{\partial^4 w_b}{\partial x^4} - H_{11}^s\frac{\partial^4 w_s}{\partial x^4} + A_{55}^s\frac{\partial^2 w_s}{\partial x^2} = I_0\left(\ddot{w}_b + \ddot{w}_s\right) + J_1\frac{d\ddot{u}_0}{dx} - J_2\frac{d^2\ddot{w}_b}{dx^2} - K_2\frac{d^2\ddot{w}_s}{dx^2} \tag{29}$$

where, A_{11}, D_{11}, etc. are the stiffnesses of the beam, and defined as:

$$(A_{11}, B_{11}, D_{11}, B_{11}^s, D_{11}^s, H_{11}^s) = \int_{-\frac{h}{2}}^{\frac{h}{2}} Q_{11}\left(1, z, z^2, f(z), zf(z), f^2(z)\right)dz \tag{30}$$

and

$$A_{55}^s = \int_{-\frac{h}{2}}^{\frac{h}{2}} Q_{55}[g(z)]^2 dz \tag{31}$$

2.3 Analytical Solution

In the current research, the FG beam is supposed to have simply supported ends. Therefore, the Navier solution technique was used, and the displacement variables are provided by:

$$\left\{ \begin{array}{c} u_0 \\ w_b \\ w_s \end{array} \right\} = \sum_{m=1}^{\infty} \left\{ \begin{array}{c} U_m \cos(\lambda x) e^{i\omega t} \\ W_{bm} \sin(\lambda x) e^{i\omega t} \\ W_{sm} \sin(\lambda x) e^{i\omega t} \end{array} \right\} \tag{32}$$

where, U_m, W_{bm}, and W_{sm} are arbitrary parameters to be calculated, ω is the natural frequency of the FG beam, and $\sqrt{i}$=-1 is the imaginary unit.

$$\lambda = m\pi / L \tag{33}$$

The following equations were derived by substituting the expansions of u_0, w_b, and w_s from Eq. (32) into the equations of motion Eqs. (27)-(29).

$$\left(\left[\begin{array}{ccc} a_{11} & a_{12} & a_{13} \\ a_{12} & a_{22} & a_{23} \\ a_{13} & a_{23} & a_{33} \end{array} \right] - \omega^2 \left[\begin{array}{ccc} m_{11} & m_{12} & m_{13} \\ m_{12} & m_{22} & m_{23} \\ m_{13} & m_{23} & m_{33} \end{array} \right] \right) \left\{ \begin{array}{c} U_m \\ W_{bm} \\ W_{sm} \end{array} \right\} = \left\{ \begin{array}{c} 0 \\ 0 \\ 0 \end{array} \right\} \tag{34}$$

where,

$$\begin{aligned} a_{11} &= A_{11}\lambda^2 \\ a_{12} &= -B_{11}\lambda^3 \\ a_{13} &= -B^s_{11}\lambda^3 \\ a_{22} &= D_{11}\lambda^4 \\ a_{23} &= D^s_{11}\lambda^4 \\ a_{33} &= H^s_{11}\lambda^4 + A^s_{55}\lambda^2 \end{aligned} \tag{35}$$

and

$$\begin{aligned} m_{11} &= I_1 \\ m_{12} &= -I_2\lambda \\ m_{13} &= -I_3\lambda \\ m_{22} &= I_1 + I_4\lambda^2 \\ m_{23} &= I_1 + I_5\lambda^2 \\ m_{33} &= I_1 + I_6\lambda^2 \end{aligned} \tag{36}$$

3 Numerical Results and Discussions

This section focuses on the current situation using numerical examples. Comparisons were conducted to demonstrate the existing formulations' validity, and the following dimensionless parameters were applied:

$$\Omega = \frac{\omega L^2}{h} \sqrt{\frac{\rho_m}{E_m}} \tag{37}$$

where, Ω is the dimensionless natural frequency (DNF).

3.1 Comparison Studies

Table 1 shows the comparison of dimensionless fundamental natural frequencies (DFNFs) of FGP beams versus p for two different α with those proposed in studies by Avcar et al. [25] and Pandey and Pradyumna [26]. The material properties were taken from the related studies, and the span-to-depth ratio (L/h=10) was employed.

Table 2 presents the comparison of DFNFs of FG beams versus different L/h with those proposed by several researchers [25, 27, 28]. The material properties were taken from the associated studies as E_m=70 GPa; ρ_m=2700 kg/m^3; E_c=380 GPa; ρ_c=3800 kg/m^3; v_m=v_c=0.23; p=0.3, as well as DNF, which was defined as Ω=$\omega L^2/h\sqrt{I_0/A_{11}}$. DFNF of FG beams increased with the increase of L/h. Additionally, at the value of L/h=100, DFNF values were identical with the results of previous works.

Table 1. Comparison of DFNFs of FGP beams versus p for two different α

α	Reference	p			
		0.5	**1**	**2**	**5**
0.1	This study	4.5920	4.0717	3.5990	3.3373
	[25]	4.5900	4.0675	3.5917	3.3260
	[26]	4.4935	4.0001	3.5647	3.3328
0.2	This study	4.5776	3.9415	3.2858	2.8591
	[25]	4.5752	3.9364	3.2769	2.8429
	[26]	4.3664	3.8138	3.2914	2.9429

Table 2. Comparison of DFNFs of FG beams versus L/h

BCs	Reference	$L/h = 10$	$L/h = 30$	$L/h = 100$
S-S	This study	2.703	2.738	2.742
	[27]	2.695	2.737	2.742
	[28]	2.702	2.738	2.742
	[25]	2.702	2.738	2.742

Table 3. Comparison of DFNFs of FG beams versus p

Mode	Reference	p					
		0	**1**	**2**	**5**	**10**	∞
1	This study	5.1529	4.0030	3.6469	3.4270	3.2993	2.6933
	[29]	5.1528	3.9716	3.5979	3.3743	3.26534	2.6773
	[30]	5.1542	3.9914	3.6267	3.4000	3.2814	2.6781
	[25]	5.1531	3.9907	3.6263	3.3998	3.2811	2.6775

Table 3 compares the DFNFs of FG beams versus p with those proposed by several researchers [25, 29, 30]. The material properties taken from the related studies, such as L/h=5, and α=0, were considered. DFNFs became lower with the increase of p. The biggest decrease of DFNF occurred between p values of 0 and 1, as shown in Table 3.

Figure 3 compares the first three modes of the DNFs of all three types of FG beams for L/h=5, p=2, and α=0.2. It can be concluded that as the Mode Numbers (MNs) increased, the DNFs also increased, and the most significant increase in DNFs occurred between MNs 1 and 2, followed by a smaller increase between MNs 2 and 3. The DNFs were highest for P and lowest for IP-I beams in all MNs. Additionally, the largest overall change in DNF was observed is the **P** beam.

Figure 4 shows DFNFs of FGP beams versus α for L/h=5, and p=2. According to Figure 4, the DFNFs decrease with respect to the increase of α, and the difference gets more pronounced for model IP-I than IP-II. Furthermore, at higher values of α, the difference of DFNFs is higher.

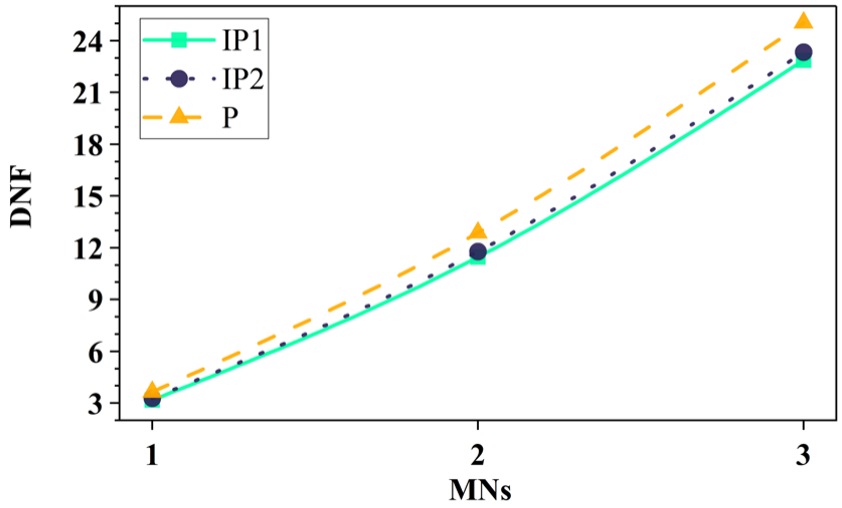

Figure 3. Variation of DNFs of P/ IP-I/ IP-II FG beams versus the first three MNs

Figure 5 shows the value of DFNFs of all three types of FG beams versus p for L/h=10, and α=0.1. With the increase of p, DFNF values decreased. The DFNFs of the FG P-type beam were higher than those of the IP-I and IP-II beams for larger values of p. Additionally, the impact of the change in p on DFNFs is most pronounced for the IP-I and least for **P**.

Figure 6 demonstrates DFNFs of all three types of FG beams versus L/h for p=2, and α=0.1. It can be concluded that with the increase of L/h ratio, DFNFs increased; and the change of DFNFs decreased. DFNFs of IP-I and IP-II became closer for higher values of L/h.

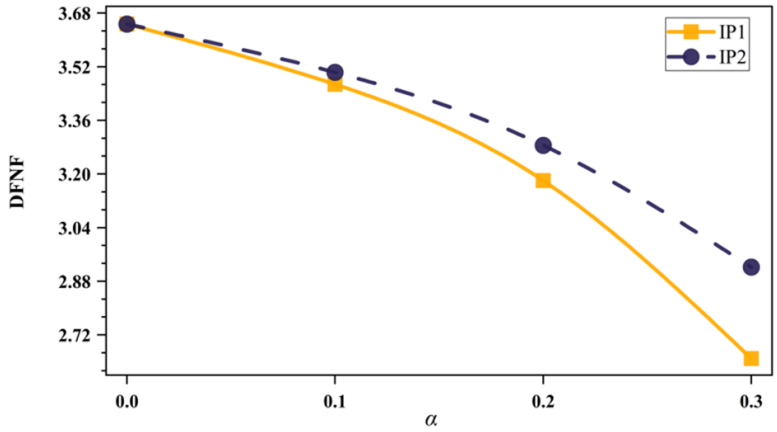

Figure 4. Variation of DFNFs of IP-I/IP-II FG beams versus α

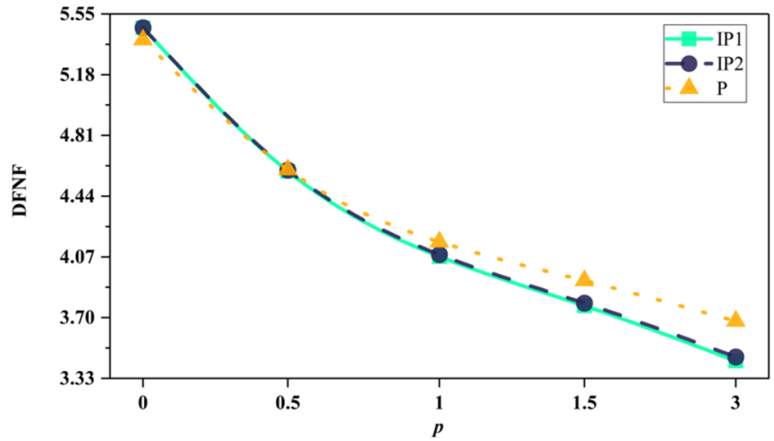

Figure 5. Variation of DFNFs of P/IP-I/IP-II FG beams versus p

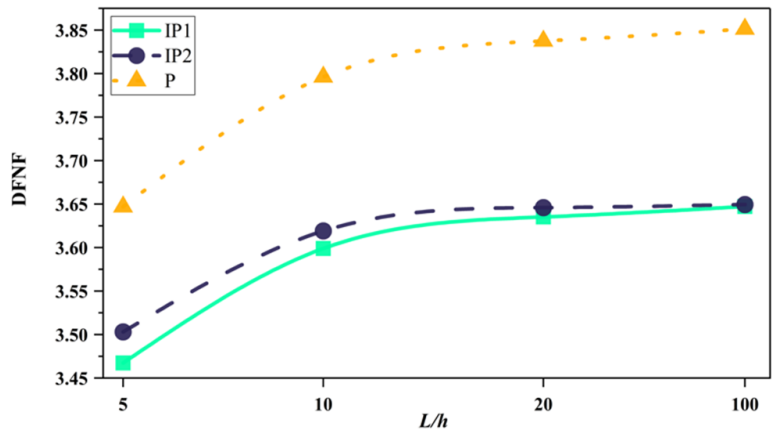

Figure 6. Variation of DFNFs of P/IP-II/IP-II FG beams versus L/h ratio

4 Conclusion

In this study, the free vibration behavior of FG beams with different porosity distribution types was studied. HSDT was employed to describe the kinematic relations of shear-deformable FG beams, while Hamilton's principle was used to derive the equations of motion. Navier's method was implemented to obtain a solution for the free vibration analysis of the FG beam under simply supported boundary conditions. The accuracy of the formulation was validated through comparison with existing studies.

The results obtained from the current study allow the following conclusions to be made:

a) The fundamental frequencies of FG beams are inversely related to p.

b) The fundamental frequencies of FG beams are inversely related to α.

c) The increase of L/h leads to an increase in the fundamental frequency.

d) The type of porosity becomes less noticeable at higher values of L/h.

e) The effect of change in p on natural frequencies is more pronounced in the porous beams rather than perfect beams.

Based on the conclusions, porosity holds potential for future works for FGMs.

Data Availability

The data used to support the research findings are available from the corresponding author upon request.

Conflicts of Interest

The authors declare no conflict of interest.

References

[1] M. Koizumi, "FGM activities in Japan," *Compos. B Eng.*, vol. 28, no. 1-2, pp. 1–4, 1997. https://doi.org/10.1016/S1359-8368(96)00016-9

[2] E. Dubovikov, D. Fomin, N. Guseva, I. Kondakov, E. Kruychkov, I. Mareskin, and A. Shanygin, "Manufacturing aspects of creating low-curvature panels for prospective civil aircraft," *Aerospace*, vol. 6, no. 2, p. 18, 2019. https://doi.org/10.3390/aerospace6020018

[3] N. D. Nguyen, T. N. Nguyen, T. K. Nguyen, and T. P. Vo, "A new two-variable shear deformation theory for bending, free vibration and buckling analysis of functionally graded porous beams," *Compos. Struct.*, vol. 282, no. 115095, 2022. https://doi.org/10.1016/j.compstruct.2021.115095

[4] H. A. Ait Atmane, A. Tounsi, and F. Bernard, "Effect of thickness stretching and porosity on mechanical response of a functionally graded beams resting on elastic foundations," *Int. J. Mech. Mater. Des.*, vol. 13, pp. 71–84, 2017. https://doi.org/10.1007/s10999-015-9318-x

[5] Y. Liu, S. Su, H. Huang, and Y. Liang, "Thermal-mechanical coupling buckling analysis of porous functionally graded sandwich beams based on physical neutral plane," *Compos. B Eng.*, vol. 168, pp. 236–242, 2019. https://doi.org/10.1016/j.compositesb.2018.12.063

[6] Y. Obata and N. Noda, "Optimum material design for functionally gradient material plate," *Arch. Appl. Mech.*, vol. 66, pp. 581–589, 1996. https://doi.org/10.1007/BF00808146

[7] J. Andertová, R. Tláskal, M. Maryška, and J. Havrda, "Functional gradient alumina ceramic materials – Heat treatment of bodies prepared by slip casting method," *J. Eur. Ceram. Soc.*, vol. 27, no. 2-3, pp. 1325–1331, 2007. https://doi.org/10.1016/j.jeurceramsoc.2006.04.088

[8] D. Chen, J. Yang, and S. Kitipornchai, "Free and forced vibrations of shear deformable functionally graded porous beams," *Int. J. Mech. Sci.*, vol. 108, pp. 14–22, 2016. https://doi.org/10.1016/j.ijmecsci.2016.01.025

[9] M. Naebe and K. Shirvanimoghaddam, "Functionally graded materials: A review of fabrication and properties," *Appl. Mater. Today*, vol. 5, pp. 223–245, 2016. https://doi.org/10.1016/j.apmt.2016.10.001

[10] M. Herrmann and W. Sobek, "Functionally graded concrete: Numerical design methods and experimental tests of mass-optimized structural components," *Struct. Concr.*, vol. 18, no. 1, pp. 54–66, 2017. https://doi.org/10.1002/suco.201600011

[11] F. Xu, X. Zhang, and H. Zhang, "A review on functionally graded structures and materials for energy absorption," *Eng. Struct.*, vol. 171, pp. 309–325, 2018. https://doi.org/10.1016/j.engstruct.2018.05.094

[12] A. A. Daikh and A. M. Zenkour, "Effect of porosity on the bending analysis of various functionally graded sandwich plates," *Mater. Res. Express*, vol. 6, no. 6, p. 065703, 2019. https://doi.org/10.1088/2053-1591/ab0971

[13] A. M. Zenkour, "A quasi-3D refined theory for functionally graded single-layered and sandwich plates with porosities," *Compos. Struct.*, vol. 201, pp. 38–48, 2019. https://doi.org/10.1016/j.compstruct.2018.05.147

[14] E. Njim, S. H. Bakhi, and M. Al-Waily, "Experimental and numerical flexural properties of sandwich structure with functionally graded porous materials," *Eng. and Technol. J.*, vol. 40, no. 1, pp. 137–147, 2022. http://doi.org/10.30684/etj.v40i1.2184

[15] M. Babaei, F. Kiarasi, K. Asemi, and M. Hosseini, "Functionally graded saturated porous structures: A review," *J. Comput. Appl. Mech.*, vol. 53, no. 2, pp. 297–308, 2022. https://doi.org/10.22059/jcamech.2022.342710.719

[16] D. Chen, K. Gao, J. Yang, and L. Zhang, "Functionally graded porous structures: Analyses, performances, and applications–A review," *Thin-Walled Struct.*, vol. 191, p. 111046, 2023. https://doi.org/10.1016/j.tws.2023.111046

[17] N. Wattanasakulpong and V. Ungbhakorn, "Linear and nonlinear vibration analysis of elastically restrained ends FGM beams with porosities," *Aerosp. Sci. Technol.*, vol. 32, no. 1, pp. 111–120, 2014. https://doi.org/10.1016/j.ast.2013.12.002

[18] Ṡ. D. Akbaś, "Forced vibration analysis of functionally graded porous deep beams," *Compos. Struct.*, vol. 186, pp. 293–302, 2018. https://doi.org/10.1016/j.compstruct.2017.12.013

[19] M. Heshmati and F. Daneshmand, "A study on the vibrational properties of weight-efficient plates made of material with functionally graded porosity," *Compos. Struct.*, vol. 200, pp. 229–238, 2018. https://doi.org/10.1016/j.compstruct.2018.05.099

[20] J. Yang and H. Shen, "Vibration characteristics and transient response of shear-deformable functionally graded plates in thermal environments," *J. Sound Vib.*, vol. 255, no. 3, pp. 579–602, 2002. https://doi.org/10.1006/jsvi.2001.4161

[21] M. H. Ghayesh, "Nonlinear vibration analysis of axially functionally graded shear-deformable tapered beams," *Appl. Math. Model.*, vol. 59, pp. 583–596, 2018. https://doi.org/10.1016/j.apm.2018.02.017

[22] N. Wattanasakulpong and A. Chaikittiratana, "Flexural vibration of imperfect functionally graded beams based on timoshenko beam theory: Chebyshev collocation method," *Meccanica*, vol. 50, pp. 1331–1342, 2015. https://doi.org/10.1007/s11012-014-0094-8

[23] M. Avcar, L. Hadji, and Ö. Civalek, "Natural frequency analysis of sigmoid functionally graded sandwich beams in the framework of high order shear deformation theory," *Compos. Struct.*, vol. 276, p. 114564, 2021. https://doi.org/10.1016/j.compstruct.2021.114564

[24] J. N. Reddy, *Mechanics of Laminated Composite Plates and Shells: Theory and Analysis*. CRC Press, 2003.

[25] M. Avcar, L. Hadji, and R. Akan, "The influence of Winkler-Pasternak elastic foundations on the natural frequencies of imperfect functionally graded sandwich beams," *Geomech. Eng.*, vol. 31, no. 1, pp. 99–112, 2022. https://doi.org/10.12989/GAE.2022.31.1.099

[26] S. Pandey and S. Pradyumna, "Thermal shock response of porous functionally graded sandwich curved beam using a new layerwise theory," *Mech. Based Des. Struct. Mach.*, vol. 51, no. 4, pp. 2055–2079, 2021. https://doi.org/10.1080/15397734.2021.1888297

[27] S. A. Sina, H. M. Navazi, and H. Haddadpour, "An analytical method for free vibration analysis of functionally graded beams," *Mater. Des.*, vol. 30, no. 3, pp. 741–747, 2009. https://doi.org/10.1016/J.MATDES.2008.05.015

[28] M. Şimşek, "Vibration analysis of a functionally graded beam under a moving mass by using different beam theories," *Compos. Struct.*, vol. 92, no. 4, pp. 904–917, 2010. https://doi.org/10.1016/j.compstruct.2009.09.030

[29] T. P. Vo, H. T. Thai, T. K. Nguyen, A. Maheri, and J. Lee, "Finite element model for vibration and buckling of functionally graded sandwich beams based on a refined shear deformation theory," *Eng. Struct.*, vol. 64, pp. 12–22, 2014. https://doi.org/10.1016/j.engstruct.2014.01.029

[30] A. S. Sayyad and Y. M. Ghugal, "Analytical solutions for bending, buckling, and vibration analyses of exponential functionally graded higher order beams," *Asian J. Civ. Eng.*, vol. 19, pp. 607–623, 2018. https://doi.org/10.1007/s42107-018-0046-z